Journal of Neuroscience Methods 226 (2014) 132–138

Journal of Neuroscience Methods

journal homepage: www.elsevier.com/locate/jneumeth

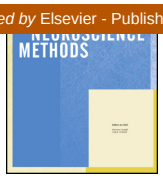

Basic Neuroscience

Molecular susceptibility weighted imaging of the glioma rim in a mouse model

Barbara Blasiak[a,b], James Landry[a], Randy Tyson[c], Jonathan Sharp[c], Umar Iqbal[g], Abedelnasser Abulrob[f,g], David Rushforth[a], John Matyas[d], Dragana Ponjevic[d], Garnette R. Sutherland[a], Stefan Wolfsberger[e], Boguslaw Tomanek[a,b,h,*]

[a] Department of Clinical Neurosciences, University of Calgary, 3330 Hospital Drive NW, Calgary, Alberta T2N 4N1, Canada
[b] Polish Academy of Sciences, Institute of Nuclear Physics, Krakow, 152 Radzikowskiego, Krakow, Malopolska 31-342, Poland
[c] Alberta Innovates Technology Futures, Calgary, Alberta, Canada
[d] Faculty of Veterinary Medicine, University of Calgary, 3330 Hospital Drive NW, Calgary, Alberta T2N 4N1, Canada
[e] Department of Neurosurgery, Medical University Vienna – General Hospital (AKH), Waehringer Guertel 18-20, 1097 Vienna, Austria
[f] Department of Cellular and Molecular Medicine, Faculty of Medicine, University of Ottawa, 451 Smyth Road, Ottawa, Ontario K1H 8M5, Canada
[g] Human Health Therapeutics Portfolio, National Research Council Canada, Ottawa, Ontario K1A 0R6, Canada
[h] Thunder Bay Regional Research Institute, 980 Oliver Road, Thunder Bay, Ontario P7B 6V4, Canada

HIGHLIGHTS

- Nanoparticles functionalized with IGFBP7-sdAb injected into mouse bind to glioma.
- Superparamagnetic iron oxide provides opportunities for application of glioma SWI.
- SWI showed better contrast-to-noise ratio for tumor rim and core than gradient echo.
- SWI combined with targeted nanoparticles provides improved glioma visualization.

GRAPHICAL ABSTRACT

SWI of the glioma before (A) and (B) after injection of the targeted contrast agent.

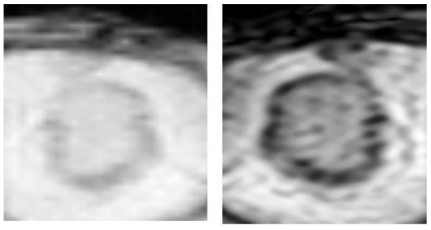

ARTICLE INFO

Article history:
Received 3 October 2013
Received in revised form 9 January 2014
Accepted 31 January 2014

Keywords:
SWI
Molecular MRI
Targeted contrast agents
Glioma

ABSTRACT

Background: Glioma is the most common and most difficult to treat brain cancer. Despite many efforts treatment, efficacy remains low. As neurosurgical removal is the standard procedure for glioma, a method, allowing for both early detection and exact determination of the location, size and extent of the tumor, could improve a patient's positive response to therapy.
New method: We propose application of susceptibility weighted molecular magnetic resonance imaging using, targeted contrast agents, based on superparamagnetic iron oxide nanoparticles, for imaging of the, glioma rim, namely brain-tumor interface. Iron oxide attached to the targeted cells increases, susceptibility differences at the boundary between tumor and normal tissue, providing the opportunity, to utilize susceptibility weighted imaging for improved tumor delineation. We investigated potential, enhancement of the tumor-brain contrast, including tumor core and rim when using susceptibility, weighted MRI for molecular imaging of glioma.
Results: There were significant differences in contrast-to-noise ratio before, 12 and 120 min after contrast, agent injection between standard gradient echo pulse sequence and susceptibility weighted molecular, magnetic resonance imaging for the core-brain, tumor rim-core and tumor rim-brain areas.

* Corresponding author at: Department of Clinical Neurosciences, University of Calgary, 3330 Hospital Drive NW, Calgary, Alberta T2N 4N1, Canada. Tel.: +1 4032213222.
E-mail address: btomanek@ucalgary.ca (B. Tomanek).

0165-0270
http://dx.doi.org/10.1016/j.jneumeth.2014.01.034

Comparison with existing methods: Currently, the most common MRI contrast agent used for glioma diagnosis is a non-specific, gadolinium-based agent providing T1-weighted enhancement. Susceptibility-weighted magnetic, resonance imaging is much less efficient when no targeted superparamagnetic contrast agents are, used.
Conclusion: The improved determination of glioma extent provided by SWI offers an important new tool for, diagnosis and surgical planning.

1. Introduction

Brain tumors are among the most devastating cancers. Among them glioblastoma is both the most common and most difficult to treat (Rock et al., 2012; Colman et al., 2009; Ohagak et al., 2005). The mean survival rate is about 50 weeks and has essentially remained unchanged over the past 30 years (Ellegala et al., 2003; Aghi et al., 2005). This poor prognosis may be related to insufficient differentiation of normal brain and tumor, thus resulting in incomplete resection. The determination of exact tumor size and its extent is important for accurate treatment planning, both for surgery and adjuvant radiotherapy (Cai and Chen, 2008). The surgical removal of malignant glioma remains the standard of practice, even though it has had only limited success due to local recurrence. The glioma rim (i.e. tumor-brain interface) is comprised of peritumoral parenchyma (Villalba et al., 2008; Blasiak et al., 2010) and provides the oxygenation and nutritional supply needed for tumor growth and to support the tumor invasion into the surrounding normal brain tissue (Vajkoczy et al., 1999). The invaded cells and the gradient-driven diffusely invasive nature of gliomas are believed to be responsible for tumor recurrence following surgery near the resection boundary (Kelly et al., 1987; Villalba et al., 2008; Jiang et al., 2008). Complete tumor removal is particularly challenging in MRI-guided treatment because standard T_1-weighted or gadolinium-enhanced MRI used for glioma diagnosis fail to precisely detect the tumor boundaries (Schwartz et al., 2006; Cai and Chen, 2008; LaConte et al., 2007; Wang et al., 2001). A clinical report comparing CT and MR imaging abnormalities to histopathology was able to establish four tumor zones (Kelly et al., 1987): zone 1 corresponding to tumor necrosis, zone 2 consisting of solid tumor tissue with increased vascularity and zones 3 and 4 corresponding to infiltrating tumor outside the area enhanced on CT and MR imaging. Changes in signal intensity using diffusion-weighted imaging, indicating restricted water diffusion, have been used to diagnose brain abscess. Molecular glioma MRI in an animal model (Gambarota et al., 2006), using targeted contrast agents, based on superparamagnetic nanoparticles (NP) conjugated to an antibody (Tomanek et al., 2012; Runge et al., 1984) have been used to target a specific tumor cell marker, potentially allowing more specific diagnosis. The most frequently used superparamagnetic NPs in molecular MRI are based on iron oxide (Lawaczeck et al., 2004), (Huber and Synthesis, 2005; Santra et al., 2005; Tomanek et al., 2012), that reduces T_2 and T_2^* relaxation times, providing tumor-specific contrast, and thus increase the capability of MRI to detect tumor boundaries (Gambarota et al., 2008; Oh et al., 2005). Iron attached to the tumor cells or tumor vasculature increases susceptibility differences at the boundary between tumor and normal tissue, providing the opportunity to utilize susceptibility weighted imaging (SWI) for improved tumor delineation. SWI has been used for diagnosis of various neurological conditions (Lupo et al., 2009; Haacke et al., 2004; Lee et al., 1999; Tong et al., 2008). In particular, SWI can detect vasculature disorders and micro-hemorrhages although its capability has not been yet fully investigated. Several investigators have shown that SWI can visualize presumed intratumoral microvasculature and necrosis (Grabner et al., 2012; Tan et al., 2000; Pinker et al., 2008; Seghal et al., 2010; Moenninghoff et al., 2010).

In our study we used gradient echo (GE) data to create SWI to investigate potential improvement in visualization of iron content in the tumor and in particular in the at the tumor-brain interface corresponding to zone 2 described by Kelly et al. (1987), using the molecular MRI of a mouse glioma model. The MRI of the mouse brain was performed before and after intravenous injection of the targeted contrast agent.

2. Materials and methods

2.1. Tumor model

Details of the tumor model have been previously described (e.g. Blasiak et al., 2010; Ellegala et al., 2003). Briefly, the U87MGdEGFRvIII cell line (U87MG), provided by the Ludwig Institute for Cancer Research (La Jolla, CA, USA), was used. Six CD-1 nude mice (male, 6 weeks old, Charles River, Canada) were used for studies. Animals were anesthetized by intraperitoneal injection of a mixture of ketamine (150 mg/kg) and xylazine (10 mg/kg) and placed in a stereotactic head frame (Kopf Instruments, Tujunga, CA). Tumor cells were inoculated by injection of approximately 5×10^4 U87MGdEGFRvIII glioma cells, suspended in a total volume of 2–3 μL, intracerebrally into the frontal lobe of each mouse with a chromatography syringe at a depth of 2.5–3 mm (1 mm anterior and 1.8 mm lateral to the bregma) (Ellegala et al., 2003). Subsequently, the bony calvarium was sealed by a droplet of bone wax to prevent reflux and the skin was sutured. After the surgery, animals were allowed to recover from anesthesia and were placed in their cages. All animal procedures were approved by the local Animal Care Committee.

2.2. MRI protocol

The MRI sessions started 10 days after cell inoculation when tumor was about 2 mm in diameter. A 9.4 T/21 cm horizontal bore magnet (Magnex, UK) with a Biospec console (Bruker, Germany) was used. A volume (3 cm diameter, 2.5 cm long) radio-frequency coil was placed over the animal's head covering the region of interest, namely the frontal cortices. For in vivo MRI experiments, a 2 mg Fe/ml concentration of the functionalized contrast agent was used (Gambarota et al., 2008) and 200 μl of the contrast agent was slowly (2–3 min) administered via tail vein cannula made of drawn down PE10 polyethylene tubing using a 0.5-ml insulin syringe with a 27-G fixed needle (vehicle, 0.9% saline).

The axial T_2^*-weighted GE images were collected at the level of the tumor before, 12 min and 2 h after contrast injection with the following parameters: FOV = 2 × 2 cm, slice thickness of 1 mm, matrix size 128 × 128, TR = 50 ms, 50 kHz bandwidth and a 15 degree flip angle; echo time (TE) was 7 ms, 10 accumulations.

The SW images were processed as described by Haacke et al. (2009). The raw time-domain data were zero filled to 512 × 512 prior to 2D Fourier transformation and a phase image generated in the frequency domain. A high-pass filter was used to remove the low-spatial-frequency phase as follows: the central 48 × 48 points were used to create a phase image which was then used to subtract out the low-frequency phase components of the original 512 × 512 phase image. An image mask was then calculated to multiply the

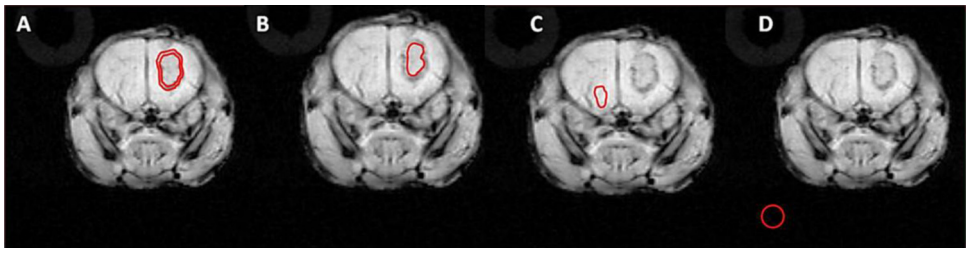

Fig. 1. Selection of regions of interest for CNR calculations: tumor rim (A), tumor core (B), normal brain (C), noise (D).

512×512 magnitude image using the following rule designed to enhance pixels of positive phase:

$$f(x,y) = \frac{\pi - \varphi(x,y)}{\pi} \quad \text{for } \pi > \varphi(x,y) > 0$$

$$f(x,y) = 1, \quad \text{otherwise}$$

This mask was multiplied with the original magnitude image four times to produce an image with enhanced contrast.

2.3. Contrast agent synthesis and injection

Commercially available iron oxide NPs were used (Nanotech-Ocean, USA). The NP consisted of a 20 nm mean diameterFe_3O_4core, embedded in a dextran matrix, with a hydrodynamic diameter of about 63 nm (Corot et al., 2006; Suwa et al., 1998). The NPs were functionalized with IGFBP7-sdAb (Hamzah et al., 2009), an antibody that binds with high specificity to the glioma vasculature. Intravenous tail injection was used to deliver the contrast agent.

2.4. Selection of regions of interest (ROI)

To analyze the tumor rim contrast-to-noise ratio (CNR), three regions of interest (ROIs) were selected for quantitative comparison (Fig. 1): tumor rim, tumor core, normal brain. Noise was calculated as average signal intensity outside of the brain.

The tumor rim was defined by the hypo-intense peripheral edges of the tumor (Fig. 1A). The tumor core was defined as the inner homogenous section of the tumor excluding the rim (Fig. 1B). The area of normal brain was selected from the artifact free area located in the contralateral hemisphere (Fig. 1C). Average signal intensities (SI) and standard deviations (SD) for each ROI were calculated (Marevisi, NRC, Canada). CNR for each ROI was calculated to quantify the differences in visualization of the rim and tumor according to the formulae:

$$\mathrm{CNR}(1) = \frac{\mathrm{SI(normal\,brain)} - \mathrm{SI(core)}}{\mathrm{Noise}}$$

$$\mathrm{CNR}(2) = \frac{\mathrm{SI(normal\,brain)} - \mathrm{SI(rim)}}{\mathrm{Noise}}$$

$$\mathrm{CNR}(3) = \frac{\mathrm{SI(core)} - \mathrm{SI(rim)}}{\mathrm{Noise}}$$

Statistical analysis was performed using ANOVA and 2-tailed Student paired t test. Data were reported as mean ± SD.

2.5. Histology

At the end of the MRI experiment, mice were sacrificed by intracardiac perfusion with heparinized saline and their brains were excised and fixed in formalin. Coronal sections (50 μm) were produced using a Vibratome sectioning instrument (Ted Pella, Redding, CA, USA). Brain tissue sections were examined for the presence of iron nanoparticles by an Iron Stain Kit (Sigma) as per manufacturer's instructions. Briefly, the sections were incubated for 30 min at room temperature with iron staining solution (a 1:1 mixture of 4% potassium ferrocyanide and 4% hydrochloric acid). Sections were then washed in deionized water and incubated for 3 min with 1% pararosaniline solution diluted 1/50 in water, followed by additional washing with deionized water. Tissue sections were then mounted on Superfrost Plus microscope slides (Fisher Scientific, Nepean, ON, Canada), cover slipped using mounting media and examined under a light microscope.

3. Results

Fig. 2 shows SWI of a mouse bearing brain tumor before (2A), 12 (2B) and 120 min (2C) after injection of the contrast agent. Respective GE images are shown for comparison in the bottom row. The tumor is not clearly visible before injection in both SWI and GE (Fig. 2A and D). SWI 12 and 120 min after injection show higher tumor and rim contrast than GE MRI.

The SW image (Fig. 3) shows noticeable visual post-contrast enhancement. The tumor core, and in particular tumor boundaries, are visibly darker when compared to the pre-contrast images.

CNR for brain tissue and tumor core in SW and GE images before, 12 and 120 min after injection of the contrast agent is shown in Fig. 4. The results show significant ($p < 0.01$) increase of CNR in SWI (from -4.3 ± 7.8 to 17.4 ± 10.2) before and 12 min post injection; no significant ($p > 0.05$) increase between before and 120 min after ($-4.3 \pm 7.7$and 2.5 ± 1.9 respectively) and significant ($p < 0.01$) decrease of CNR between 12 and 120 min after injection (from 17.4 ± 10.2 to 2.5 ± 1.9). GE shows CNR values of -0.9 ± 2.8, 6.3 ± 5.3, 2.9 ± 1.4 corresponding to significant intensity changes for before/12 min after and before/120 min after ($p < 0.05$ in both cases). There were no significant changes between 12 and 120 min after injection ($p > 0.05$). A comparison of CNR for brain tissue and tumor core between SWI and GE showed no significant differences before and 120 min after injection ($p > 0.05$). There was a significant difference 12 min after the injection ($p < 0.05$) when CNR was about 3 times higher in SWI than in GE images (17.4 ± 10.2 and 6.3 ± 5.3).

Negative CNR (-4.3 ± 7.7; normal brain darker) between brain tissue and tumor core was observed before injection in SW images while CNR became positive 12 and 120 min after injection (17.4 ± 10.2; 2.5 ± 1.9). In GE negative CNR was also observed before injection (-0.9 ± 2.8), and become positive 12 and 120 min after injection (6.3 ± 5.3; 2.9 ± 1.4).

CNR for normal brain tissue and tumor rim in SW and GE images before, 12 and 120 min after injection of the contrast agent is shown in Fig. 5. The results show significant ($p < 0.05$) increase of CNR in SWI before and 12 min after injection (from 15.1 ± 10.9 to 35.3 ± 10.7), before and 120 min after (15.1 ± 10.9 and 20.1 ± 10.1)and between 12 and 120 min after injection (35.3 ± 10.7 and 20.1 ± 10.1) The difference in CNR in GE was not significant ($p > 0.05$) for before/12 min after, before/120 min after and 12/120 min after injection respectively with the corresponding CNR values of 7.8 ± 10.9; 16.8 ± 5.2; 11.8 ± 4.6. A comparison of

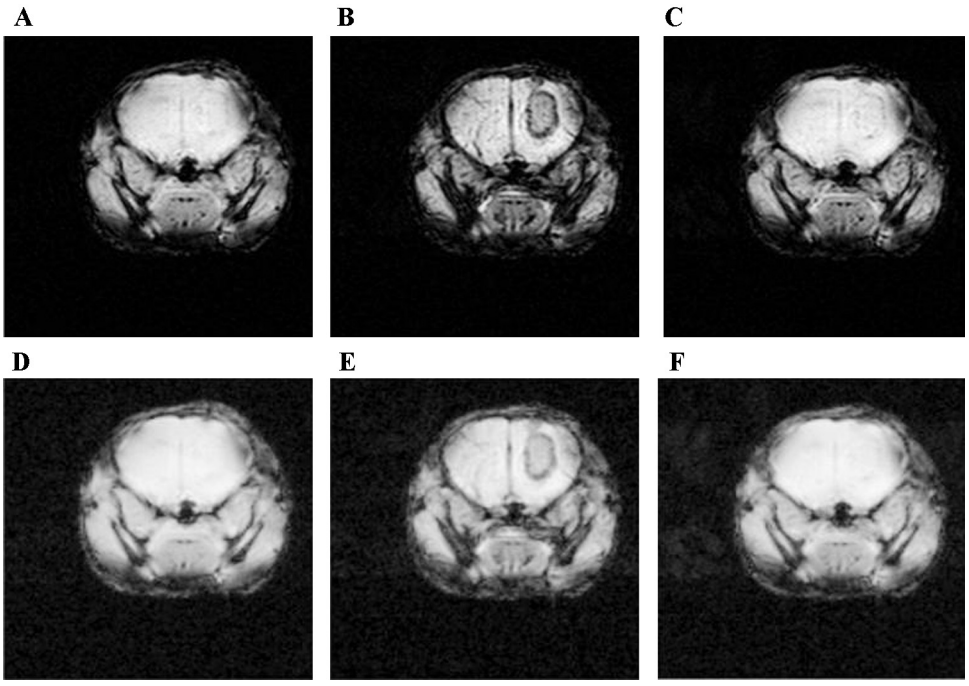

Fig. 2. SW (top row) and GE (bottom row) MR images of a mouse bearing brain tumor before (A, D), 12 (B, E) and 120 min (C, F) after injection of the targeted contrast agent.

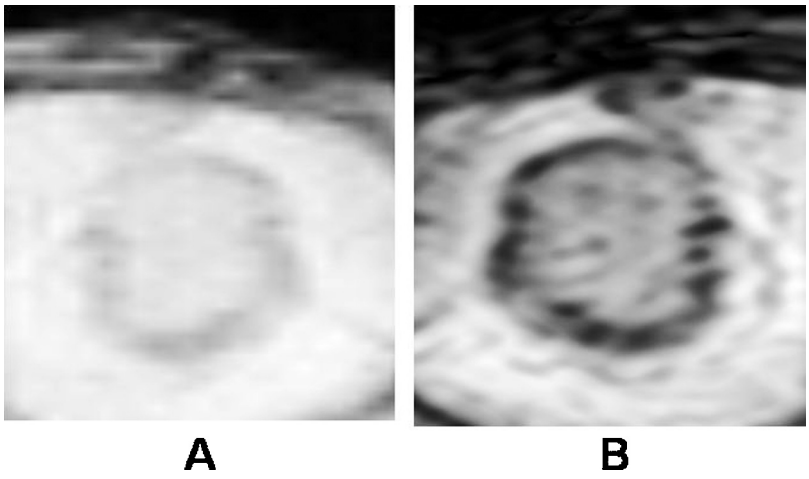

Fig. 3. Magnified SWI of the glioma including rim and core obtained before (A) and 12 min (B) after injection of the targeted contrast agent.

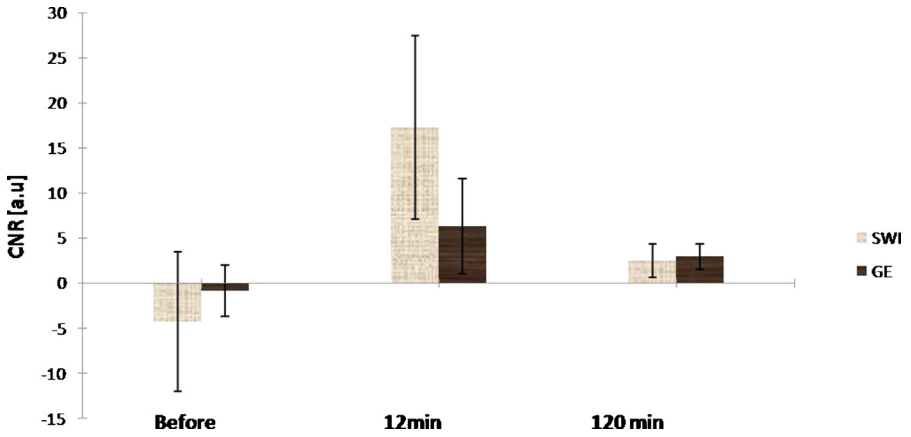

Fig. 4. A comparison of CNR for brain tissue and tumor core using SW and GE images before, 12 and 120 min after injection of the contrast agent.

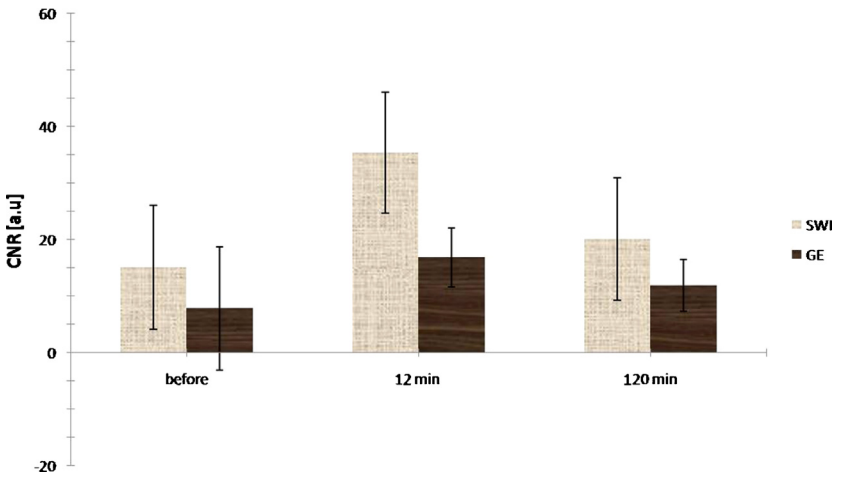

Fig. 5. A comparison of CNR for brain tissue and tumor rim in SW and GE images before, 12 and 120 min after injection of the targeted contrast agent.

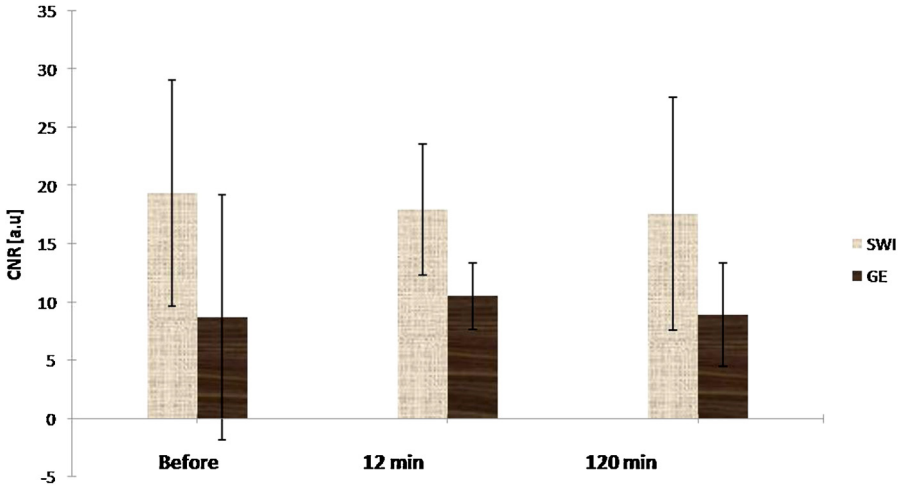

Fig. 6. A comparison of CNR for tumor core and tumor rim in SW and GE images before, 12 and 120 min after injection of the contrast agent.

CNR for normal brain tissue and tumor rim between SWI and GE showed significant differences before ($p < 0.04$), 12 min ($p < 0.01$) and 120 min ($p < 0.03$) after injection

CNR for tumor rim and tumor core in SW and GE images before, 12 and 120 min after injection of the contrast agent is shown in Fig. 6. The results show no significant ($p > 0.05$) change of CNR (from 19.4 ± 9.7 to17.7 ± 5.6) in SWI before and 12 min after injection; no significant ($p > 0.05$) change between before and 120 min after (from 19.4 ± 9.7 to 17.6 ± 10.0) and no significant ($p > 0.05$) change of CNR between 12 and 120 min after injection (from 17.7 ± 5.6 to 17.6 ± 10.0). GE shows similar tendency ($p > 0.05$) for before/12 min after, before/120 min after and 12/120 min after respectively with the corresponding CNR values 8.7 ± 10.5, 10.5 ± 2.8 and 8.9 ± 4.4. A comparison of CNR between SWI and GE for tumor core and rim showed significant ($p < 0.05$) differences at each time point. CNR for tumor rim and corein both SWI and GE was positive at each time point.

Histological images (Fig. 7) of the brain sections obtained 24 h after contrast injection confirmed higher accumulation of the iron oxide within the rim when compared to the tumor core and non-tumor region. Our results have not provided information if the tumor cells or tumor microvasculature were present outside the rim. However the extend of the tumor has been a topic of recent studies by others (Wang and Zhou, 2012; Iqbal et al., 2010).

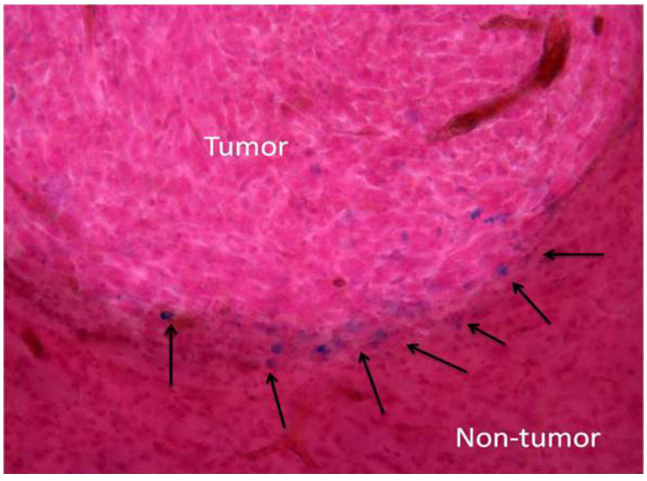

Fig. 7. Microscopic images of mouse glioma sections obtained using Prussian Blue staining collected after the last MRI session (24 h after intravenous injection of the targeted contrast agent). The images show accumulation of the iron within the tumor (as indicated by the black arrow). Blue spots indicate iron, red – nuclei and pink – cytoplasm. (For interpretation of the references to color in this figure legend, the reader is referred to the web version of the article.)

4. Discussion

The results showed that targeted NPs are not accumulating homogenously throughout the tumor region. Twelve min after contrast injection CNR was improved for the tumor rim and brain tissue as well for the tumor core and brain tissue in both SW and GE images indicating higher accumulation of the NPs in the tumor rim and core region than in the brain tissue (Fig. 2). This effect was less evident in GE than in SW images as demonstrated by quantitative CNR analysis. There were significant differences in CNR before, 12 and 120 min after contrast agent injection between GE and SWI for the core-brain, tumor rim-core and tumor rim-brain areas, except tumor core-brain CNR before and 120 min after injection.

The higher CNR for SWI after NP injection when compared with GE for each of the measured regions is caused by enhanced susceptibility effects in phase sensitive SWI (Haacke et al., 2004, 2009; Weinstein et al., 2010). The decrease of signal from the normal brain, tumor core and rim 12 and 120 min after contrast injection is caused by the NPs accumulation (Weinstein et al., 2010) in all these regions. The highest CNR between tumor rim and normal brain in both SWI and GE images is caused by the highest accumulation of NPs in tumor rim followed by the accumulation in tumor core and in normal brain.

The above observations are associated with significant hypervascularization and involvement of peritumoral parenchyma adjacent to the tumor growth. The angiogenesis induces hypervascularization, which provides oxygenation and nutritional supply needed for tumor growth and supporting the tumor ability to invade the surrounding parenchyma (Vajkoczy et al., 1999). Chronic overproduction of angiogenic factors, such as VEGF, in malignant glioma leads to uncontrolled development of new blood vessels, increased vascular permeability and tumor growth (Blasiak et al., 2010). It is evident from the result of this study that the vasculature-rich rim is abnormal in SWI appearance compared to the tumor core and normal brain regions. This effect is enhanced in SWI, as it is particularly sensitive to the presence of blood vessels with superparamagnetic contrast agents. This improved determination of the glioma extent provided by SWI may be important in both diagnosis and treatment, as it would allow detection of cells outside the grossly visible mass, invading locally or metastasizing distantly (Swanson et al., 2003). Of particular interest may be the application of contrast agent enhanced SWI to intraoperative MRI. Contrast agents injected prior to surgical intervention may enhance visualization in surgical planning, intraoperative MRI or on MRI acquired during dissection. This could increase the precision of tumor resection at the vessel-rich tumor-brain interfaces. However the lack of the approved targeted NPs in patients remains a current limitation.

The rim enhancement has been observed by other authors in both T_2- and T_1-weighted imaging with Gd enhancement for MRI of abscesses and multiple sclerosis (Schwartz et al., 2006). The enhancement was attributed to the generation of paramagnetic free radicals by macrophages (Haimes et al., 1989) in either abscesses or multiple sclerosis plaques (Yetkin and Haughton, 1995). However, hypointensity was found to be non-specific (Schwartz et al., 2006). Elevated iron levels have also been reported in many neurodegenerative disorders, including Parkinson's disease, Alzheimer's disease, Huntington's disease and amyotrophic lateral sclerosis.

High-spatial resolution SWI provides complementary information on the brain vasculature, hemorrhage, and iron content due to its sensitivity to susceptibility differences (Haacke et al., 2004; Rauscher et al., 2005). Our results showed that SWI is also useful for the evaluation of tumor extent in a murine model and shows promise for evaluating clinical brain tumors by enhanced visualization of heterogeneity.

5. Conclusions

The study demonstrates that improved visualization of glioma structure can be achieved using SWI in combination with targeted iron oxide contrast agents. This technique can provide assessment of the microvascularity inside and beyond the tumor margin in the glioma animal model at 9.4 T by providing improved CNR for tumor rim, core and normal tissue. This enables improved glioma identification, characterization and detection that could be used for enhanced diagnosis, improved treatment, treatment monitoring of gliomas and possibly for a better understanding of other cerebrovascular diseases.

Acknowledgements

The work was supported by the Collaborative Health Research Project Canada (CIHR/NSERC) and the CRIO Alberta Innovates Health Solutions Grant.

References

Aghi M, Gaviani P, Henson JW, Batchelor TT, Louis DN, Barker FG. Magnetic resonance imaging characteristics predicts epidermal growth factor receptor amplification status in glioblastomas. Clin Cancer Res 2005;12(9):8600–5.

Blasiak B, Tomanek B, Abulrob A, Iqbal U, Stanimirovic D, Albaghdadi H, et al. Detection of T_2 changes in an early mouse brain tumor. Magn Reson Imaging 2010;28:784–9.

Cai W, Chen X. Multimodality molecular imaging of tumor angiogensis. J Nucl Med 2008;49:113–28.

Colman H, Zhang L, Sulman EP, McDonald JM, Shooshani NL, Rivera A, et al. A multigene factor predictor of outcome in glioblastoma. Neuro-oncol 2009;12(1):49–57.

Corot C, Robert P, Idee JM, Port M. Recent advances in iron oxide nanocrystal technology for medical imaging. Adv Drug Deliv Rev 2006;58(14):1471–504.

Ellegala DB, Leong-Poi H, Carpenter JE, Klibanov AL, Kaul S, Shaffrey ME, et al. Imaging tumor angiogenesis with contrast ultrasound and microbubbles targeted to αvß3. Circulation 2003;94:336–41.

Gambarota G, van Laarhoven HWM, Philippens M, Lok J, van der Kogel A, Punt CJA, et al. Assessment of absolute blood volume in carcinoma by USPIO contrast-enhanced MRI. Magn Reson Imaging 2006;24(3):279–89.

Gambarota G, Leenders W, Maass C, Wesseling P, van der Kogel B, van Tellingen O, et al. Characterisation of tumor vasculature in mouse brain by USPIO contrast-enhanced MRI. Br J Cancer 2008;98:1784–9.

Grabner G, Nobauer I, Elandt K, Kronnerwetter C, Trattinig S, Preusser M. Longitudinal brain imaging of five malignant glioma patients treated with bevacizumab using susceptibility-weighted magnetic resonance imaging at 7 T. Magn Reson Imaging 2012;30:139–47.

Haacke ME, Xu Y, Cheng XC, Reichenbach JR. Sucseptibility-weighted imaging (SWI). Magn Reson Med 2004;52(3):612–8.

Haacke ME, Mittal S, Wu Z, Neelavalli J, Cheng YCN. Susceptibility-weighted imaging: technical aspects and clinical applications. Am J Neuroradiol 2009;30:19–30.

Haimes AB, Zimmerman RD, Morgello S, Weingarten K, Becker RD, Jennis R, et al. MR imaging of brain absesses. Am J Roentgenol 1989;152(5):1073–85.

Hamzah J, Altin JG, Herringson T, Parish CR, Hämmerling GJ, O'Donoghue H, et al. Targeted liposomal delivery of TLR9 ligands activates spontaneous antitumor immunity in an autochthonous cancer model. J Immunol 2009;183(2):1091–8.

Huber DL. Synthesis, properties and applications of iron nanoparticles. Small 2005;1(5):482–501.

Iqbal U, Albaghdadi H, Luo Y, Arbabi M, Desvaux C, Veres T, et al. Molecular imaging of glioblastoma multiforme using anti-insulin-like growth factor-binding protein-7 single-domain antibodies. Br J Cancer 2010;103(10):1606–16.

Jiang W, Xiang C, Cazacu S, Broadie C, Mikkelson T. Insulin-like growth factor binding protein 7 mediates glioma cell growth and migration. Neoplasia 2008;10(12):1335–42.

Kelly J, Daumas-Duport C, Kispert DB, Kall BA, Scheithauer BW. Imaging-based stereotaxic serial biopsies in untreated intracranial glial neoplasms. J Neurosurg 1987;66:865–74.

LaConte LE, Nitin N, Zurkiya O, Caruntu D, O'Connor CJ, Hu X, et al. Coating thickness of magnetic iron oxide nanoparticles affects R2 relaxivity. J Magn Reson Imaging 2007;26:1634–41.

Lawaczeck R, Memzel M, Pietsch H. Superparamagnetic iron oxide particles: contrast media for magnetic resonance imaging. Appl Organomet Chem 2004;18(10):506–16.

Lee BC, Vo KD, Kido DK, Mukherjee P, Reichenbach J, Lin W, et al. MR high-resolution blood oxygenation level dependent venography of occult (low-field) vascular lesions. Am J Neuroradiol 1999;20:1239–42.

Lupo J, Banerjee S, Hammond KE, Kelley DAC, Xu D, Chang SM, et al. GRAPPA-based susceptibility-weighted imaging of normal volunteers and patients with brain tumours at 7 T. Magn Reson Imaging 2009;27(4):480–8.

Moenninghoff C, Maderwald S, Theysohn JM, Kraff O, Ladd ME, Hindy NE, et al. Imaging of adult astrocytic brain tumor with 7 T MRI: preliminary results. Eur Radiol 2010;20:704–13.

Oh J, Cha S, Aiken AH, Eric T, Han ET, Crane JC, et al. Quantitative apparent diffusion coefficients and T_2 relaxation times in characterizing contrast enhancing brain tumors and regions of peritumoral edema. J Magn Reson Imaging 2005;21(6):701–8.

Ohagak H, Kleihues P. Population-based studies on incidence, survival rates, and genetic alterations in astrocytic and oligodendroglialgliomas. J Neuropathol Exp Neurol 2005;64:479–89.

Pinker K, Noebauer-Huhmann IM, Stavrou I, Hoeftberger R, Szomolanyi P, Weber M, et al. High-field, high-resolution, susceptibility-weighted magnetic resonance imaging: improved image quality by addition of contrast agent and higher field strength in patients with brain tumors. Neuroradiology 2008;50:9–16.

Rauscher A, Sedlacik J, Barth M, Haacke EM, Reichenbach JR. Noninvasive assessment of vascular architecture and function during modulated blood oxygenation using susceptibility weighted magnetic resonance imaging. Magn Reson Med 2005;54:87–95.

Rock K, Mcardle O, Forde P, Dunne M, Fitzpatrick D, O'Neill B, et al. A clinical review of treatment outcomes in glioblastoma multiforme—the validation in a non-trial population of the results of a randomised Phase III clinical trial: has a more radical approach improved survival? Br J Radiol 2012;85(1017):729–33.

Runge VM, Clanton JA, Partian CL, James AE. Respiratory gating in magnetic resonance imaging at 0.5 Tesla. Radiology 1984;151:521–3.

Santra S, Zhang P, Wang K, Tan W. Conjugation of biomolecules with luminophore-doped silica nanoparticles for photostable biomarkers. Anal Chem 2005;22(9):4988–93.

Schwartz KM, Erickson BJ, Luccinetti C. Pattern of T_2 hypointensity associated with ring-enhancing brain lesions can help to differenciate pathology. Diagn Neuroradiol 2006;48:143–9.

Seghal V, Delproposto Z, Haddar Z, Tong KA, Wycliffe N, Kido DK, et al. Susceptibility-weighted imaging to visualize blood products and improve tumor contrast in the study of brain masses. J Magn Reson Imaging 2010;22(4):41–51.

Suwa T, Ozawa S, Ueda M, Ando N, Kitajima M. Magnetic resonance imaging of esophageal squamous cell carcinoma using magnetite particles coeated with aniti-epidermal growth factor receptor antibody. Int J Cancer 1998;75(4):626–34.

Swanson KR, Bridge C, Murray JD, Alvord EC. Virtual and real brain tumors: using mathematical modeling to quantify glioma growth and invasion. J Neurol Sci 2003;216(1):1–10.

Tan IJ, van Schijndel RA, Pouwels PJ, van Walderveen MA, Reichenbach JR, Manoliu RA, et al. MR venography of multiple sclerosis. Am J Neuroradiol 2000;21:1039–42.

Tomanek B, Iqbal U, Blasiak B, Abulrob A, Albaghdadi H, Matyas JR, et al. Evaluation of brain tumor vessels specific contrast agents for glioblastoma imaging. Neuro-oncol 2012;14(1):53–63.

Tong KA, Ashwal S, Obenause A, Nickerson JP, Kido D, Haake EM, et al. imaging:a review of clinical applications in children. Am J Neuroradiol 2008;29:36–50.

Vajkoczy P, Menger MD, Vollmar B, Schilling L, Schmiedek P, Hirth KP, et al. Inhibition of tumor growth, angiogenesis, and microcirculation by the novel Flk-1 inhibitor SU5416 as assessed by intravital multi-fluorescence videomicroscopy. Neoplasia 1999;1:31–41.

Villalba AM, Okuducu AF, Deimling A. The evolution of our understanding on glioma. Brain Pathol 2008;18:455–63.

Wang S, Zhou J. Diffusion tensor magnetic resonance imaging of rat glioma models: a correlation study of MR imaging and histology. J Comput Assist Tomogr 2012;36(6):739–44.

Wang YX, Hussain SM, Krestin GP. Superparamagnetic iron oxide contrast agents: physicochemical characteristics and applications in MR imaging. Eur Radiol 2001;11(11):2319–31.

Weinstein J, Varallyay CG, Dosa E, Gahramanov S, Hamilton B, Rooney WD, et al. Superparamagnetic iron oxide nanoparticles: diagnostic magnetic resonance imaging and potential therapeutic applications in neurooncology and central nervous. J Cereb Blood Metab 2010;30:15–35.

Yetkin AB, Haughton VM. A typical demyelinating lesions in patients with MS. Neuroradiology 1995;37:284–6.